SCIENTIFIC REPORTS

OPEN

Quantitative Mass Spectrometry Imaging Reveals Mutation Status-independent Lack of Imatinib in Liver Metastases of Gastrointestinal Stromal Tumors

Received: 11 March 2019
Accepted: 9 July 2019
Published online: 23 July 2019

Denis Abu Sammour[1,2], Christian Marsching[1,2], Alexander Geisel[1], Katrin Erich[1,2], Sandra Schulz[1,2], Carina Ramallo Guevara[1,2], Jan-Hinrich Rabe[1,2], Alexander Marx[3], Peter Findeisen[4], Peter Hohenberger[5] & Carsten Hopf[1,2]

Mass spectrometry imaging (MSI) is an enabling technology for label-free drug disposition studies at high spatial resolution in life science- and pharmaceutical research. We present the first extensive clinical matrix-assisted laser desorption/ionization (MALDI) quantitative mass spectrometry imaging (qMSI) study of drug uptake and distribution in clinical specimen, analyzing 56 specimens of tumor and corresponding non-tumor tissues from 27 imatinib-treated patients with the biopsy-proven rare disease gastrointestinal stromal tumors (GIST). For validation, we compared MALDI-TOF-qMSI with conventional UPLC-ESI-QTOF-MS-based quantification from tissue extracts and with ultra-high resolution MALDI-FTICR-qMSI. We introduced a novel generalized nonlinear calibration model of drug quantities based on computational evaluation of drug-containing areas that enabled better data fitting and assessment of the inherent method nonlinearities. Imatinib tissue spatial maps revealed striking inefficiency in drug penetration into GIST liver metastases even though the corresponding healthy liver tissues in the vicinity showed abundant imatinib levels beyond the limit of quantification (LOQ), thus providing evidence for secondary drug resistance independent of mutation status. Taken together, these findings underscore the important application of MALDI-qMSI in studying the spatial distribution of molecularly targeted therapeutics in oncology, namely to serve as orthogonal post-surgical approach to evaluate the contribution of anticancer drug disposition to resistance against treatment.

Matrix-assisted laser desorption/ionization (MALDI) mass spectrometry imaging (MSI) has emerged as a powerful label-free technology for studying spatial distributions of analytes in tissues. Owing to its high chemical specificity and ability to track hundreds of analytes simultaneously, MALDI-MSI has gained traction in various areas of biomolecular research such as quantitative profiling of metabolites, lipids, peptides, proteins and drugs[1–4]. In the latter case, MALDI-MSI has found its way into pharmaceutical research and development, where disposition of drugs and their carriers can be effectively monitored alongside their pharmacodynamics and toxic effects[4–8].

Traditionally, quantitative assessment of drug distribution in patient tissues employs bioanalytical techniques such as UPLC-ESI-MS, which assume homogenous distribution of analytes and require tissue homogenization resulting in a complete loss of spatial context[5]. In contrast, MALDI-MSI provides spatial information, and

[1]Center for Mass Spectrometry and Optical Spectroscopy (CeMOS), Mannheim University of Applied Sciences, Paul-Wittsack-Str. 10, 68163, Mannheim, Germany. [2]Institute of Medical Technology, Heidelberg University and Mannheim University of Applied Sciences, Paul-Wittsack-Str. 10, 68163, Mannheim, Germany. [3]Institute of Pathology, University Medical Center Mannheim of Heidelberg University, Mannheim, Germany. [4]Institute of Clinical Chemistry, University Medical Center Mannheim of Heidelberg University, Mannheim, Germany. [5]Division of Surgical Oncology and Thoracic Surgery, University Medical Center Mannheim of Heidelberg University, Mannheim, Germany. Denis Abu Sammour and Christian Marsching contributed equally. Correspondence and requests for materials should be addressed to C.H. (email: carsten.hopf@medtech.uni-heidelberg.de)

much effort has recently been devoted to establish quantitative MSI (qMSI) techniques[1–4,9–12]. Linear calibration based on tissue mimetic models or compound dilution series spotted onto tissue, as well as signal normalization against stable isotope-labeled internal standards (IS)[11] and the calculation of tissue extinction coefficients (TEC)[10] were introduced to compensate for the inherently high technical variability of MALDI-MSI[3,4,12]. Furthermore, advanced rational testing criteria for evaluating linearity of response, variability, reproducibility and limits of detection of qMSI have been suggested[13]. Despite these technical advances, MALDI-qMSI has not yet been widely adapted to clinical pharmacology.

In clinical oncology, the ability to monitor drug penetration into tumors constitutes a key medical need[14]. However, tumor heterogeneity and the poorly understood spatial organization of the tumor microenvironment present major challenges for drug uptake and, hence, effective cancer treatment[15,16]. This challenge has prompted qMSI studies of drug disposition and of pharmacological/toxic effects in tumor tissues and their surroundings in mice[17,18]. Most mouse studies and pioneering qualitative MSI studies of the tyrosine kinase inhibitor (TKI) erlotinib in patient tissue report high degrees of variability and intratumor heterogeneity as well as highly heterogeneous drug distribution[19–21]. However, clinical qMSI proof-of-concept studies of drug distribution are still lacking.

Here, we present the first extensive clinical MALDI-qMSI drug disposition study of a TKI, imatinib, in 56 resection specimens of tumor and surrounding non-tumor tissues from 27 patients with the biopsy-proven rare disease gastrointestinal stromal tumor (GIST). GISTs can occur throughout the gastrointestinal tract but also as a metastatic tumor elsewhere in the abdominal cavity, as well as in liver, but rarely in lungs and distant peripheral sites. GISTs being a rare disease have been estimated to occur with a frequency of 14–20 per million[22]. Imatinib is the standard first line treatment for GIST, effectively stopping autophosphorylation and tumor proliferation particularly in exon 11 mutated GIST[23–25]. However, tumors are prone to imatinib resistance, which is mainly attributed to secondary somatic mutations in the receptor tyrosine kinases KIT (CD117 or stem cell factor receptor), the gene product of the protooncogene *c-kit*, or the platelet-derived growth factor receptor alpha (PDGFRA)[26,27]. In this study, we introduce generalized nonlinear regression as a superior calibration method based on imatinib-containing pixels, report MALDI-qMSI of three full technical replicates, and compare these results [fast time of flight MALDI-TOF-qMSI and ultra-high-resolution Fourier-Transform Ion Cyclotron Resonance (FTICR-qMSI)] with conventional UPLC-ESI-QTOF-MS quantification. Taken together, our data suggests that MALDI-qMSI compares well with UPLC-ESI-QTOF-MS quantification, and that spatially resolved MS has utility in clinical pharmacology. We can demonstrate that independent of mutation status of the tumor, imatinib failed to penetrate or to be retained in tumor tissue in all GIST liver metastasis cases tested.

Results and Discussion

For successful therapy, anticancer drugs must penetrate into tumor tissue and reach their target in cancer cells at sufficient quantities. In this study, we aimed to improve computational calibration in MALDI-TOF-qMSI, to provide proof-of-concept for the utility in clinical pharmacology of this technique by rigorously comparing it with conventional UPLC-ESI-QTOF-MS-based quantification and to cast light onto the effectiveness of uptake (or lack of export or intra-tissue metabolism) of the therapeutic TKI, imatinib, into GIST tissue. We systematically examined GIST and corresponding non-tumor samples from 27 patients who received the TKI imatinib as first line treatment but presented with refractory disease. Some patients had developed metastatic lesions, mostly in the liver (Supplementary Table S1). All patients received imatinib prior to surgery according to their treatment plan (note that the elimination half-life for imatinib is approximately 16–18 h)[28], thus enabling investigation of the drug's distribution in resection specimens. Due to the limited quantities of tissue available for these samples and since all measurements were conducted in triplicates, some samples were used up completely before reaching the next round of measurements such that only samples from 18 and 5 patients were available for UPLC-ESI-QTOF-MS and MALDI-FTICR-qMSI measurements, respectively. All slides for MALDI-qMSI featured an imatinib dilution series spotted onto porcine liver tissue and a spray-coating of deuterated imatinib-D8 for lock-mass calibration and normalization, respectively (Supplementary Fig. S1).

Calibration curves and quantification of imatinib. For drug quantification, a calibration curve has to be fitted to this dilution series[4], and users typically manually encircle spots that are then used as regions of interest in computation of the calibration curve. In contrast, we computationally defined drug-bearing areas, including only pixels where the drug was detected with $S/N \geq 3$. The lower the drug concentration spotted, the more the outlines of drug-spotted areas diverge from the expected circular shape (Supplementary Fig. S3). This can lead to signal dilution and underestimation of signal intensity when the mean signal intensity includes pixels that do not carry drug signal (Supplementary Fig. S3). This effect is even more drastic in heterogeneous tumor tissue, where the drug can only be observed in few pixels.

More importantly, all drug dilution series measured either with MALDI-TOF-qMSI or MALDI-FTICR-qMSI (Supplementary Fig. S4) deviated from linearity. We therefore wondered if nonlinear regression fitting might be a better option for calibration than a linear regression fit. As illustrated for an exemplary dilution series in Fig. 1a,b, the generalized nonlinear calibration provided a much better fit indicated by the 6- and 3- fold better residual standard error (RSE) of the calibration curve for MALDI-TOF-qMSI and MALDI-FTICR-qMSI, respectively. Figure 1d indicates a significant decrease in RSE for all MALDI-TOF-qMSI calibration curves ($p < 0.0001$; $n = 48$) for the nonlinear calibration when compared to the linear one. The linear and nonlinear fits were nearly identical for UPLC-ESI-QTOF-MS calibration (Fig. 1c) indicating a true linear response of the system. This also shows the generalizability and the ability of this calibration method to not only model the calibration curves of analytes but also convey a quantitative assessment of its deviation from linearity.

The observed nonlinearity may be of particular relevance. A similar behavior has already been reported by Pirman and co-workers[11], and was attributed to the matrix-to-analyte ratio. Moreover, the complex MALDI process, non-uniform tissue-ion suppression, interferences from matrix background signals, and different ion

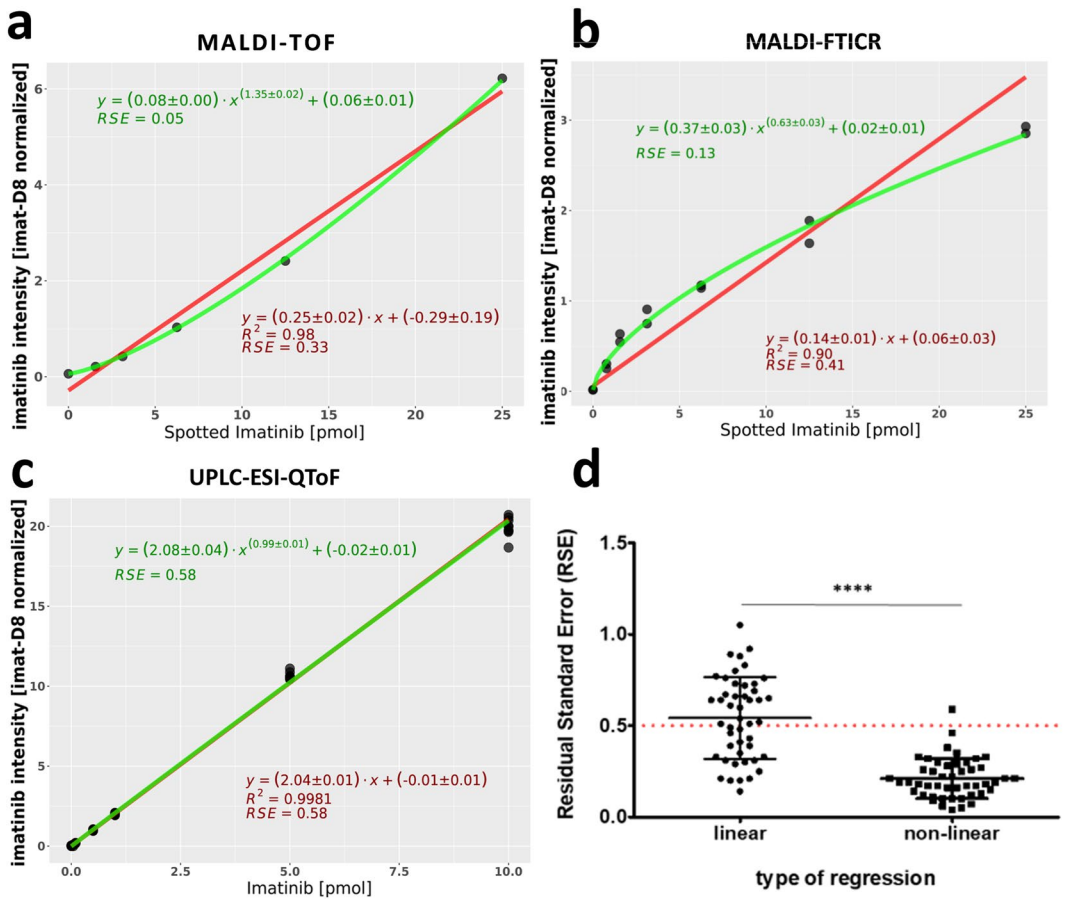

Figure 1. Generalized nonlinear regression model for calibration in qMSI. Comparison of calibration curves for a sample dataset by linear (red) and generalized nonlinear regression (green) for (**a**) MALDI-TOF-qMSI, (**b**) MALDI-FTICR-qMSI and (**c**) UPLC-ESI-QTOF-MS. Grey circles represent the mean intensity of the imatinib-containing pixel within a dilution series area. (**d**) RSE for linear and generalized nonlinear calibration curves of MALDI-TOF-qMSI.

detection/counting technologies are all factors that could contribute to nonlinear responses[29]. Even though it is common for MALDI-TOF- and –FTICR-qMSI studies to use linear calibration for drug dilution series, this linearity cannot always be guaranteed for rare heterogeneous tissue samples even with optimized matrix-to-analyte ratios[10]. Especially in the case of clinical samples screening where samples are obtained from different individuals and typically contain different amounts of target analyte, it is unlikely that any method can guarantee optimal matrix-to-analyte ratios in all scenarios and for all samples. Hence, we hypothesize here that nonlinear calibration may be a more accurate and a generally more widely applicable method, especially in clinical pharmacology. This calibration method should be evaluated by the scientific community in independent studies, in particular clinical qMSI studies. On another cautionary note, we suggests that for a reliable reporting of a drug's uptake and distribution, the level of the drug should always be reported relative to its LOQ; drawing conclusions based on low intensity MS ion images of the drug can be potentially misleading and unreliable.

Quantitative analysis of imatinib content in GIST specimens by UPLC-ESI-QTOF-MS and MALDI-qMSI. Next we systematically compared the average imatinib content in both normal and tumor tissue sections (in pmol/section) for all three full replicates using gold-standard UPLC-ESI-QTOF-MS and MALDI-TOF-qMSI (Fig. 2a,b). Also for this comparison, the mean imatinib signal intensity in MALDI-qMSI datasets was calculated solely from imatinib-containing pixels (S/N $\geq$ 3 for *m/z* 494.26; Fig. 2c).

Most tissue sections with imatinib levels above LOQ for both MS methods corresponded to normal liver tissue. In these cases, imatinib quantified by MALDI-TOF-qMSI displayed acceptable correlation with results from UPLC-ESI-QTOF-MS quantification. However, MALDI-TOF-qMSI tended to underestimate imatinib. Nevertheless, 78% of all samples, in which imatinib could be quantified, were inside a window of a 2-fold difference (grey area in Fig. 2d). MALDI-FTICR-qMSI matched the UPLC-ESI-QTOF-MS results even more closely (Fig. 2e) where 87% of all samples that reached the MALDI-FTICR-qMSI measurement round were within a 2-fold difference relative to UPLC-ESI-QTOF-MS.

In contrast to UPLC-ESI-QTOF-MS measurements that utilized extracts of entire tissue slices, MALDI-TOF- and –FTICR-qMSI add the crucial benefit of delivering spatial drug distribution maps, which - with histopathological tissue annotation - enables co-localization analysis of drugs within different tissue morphologies. Loss of

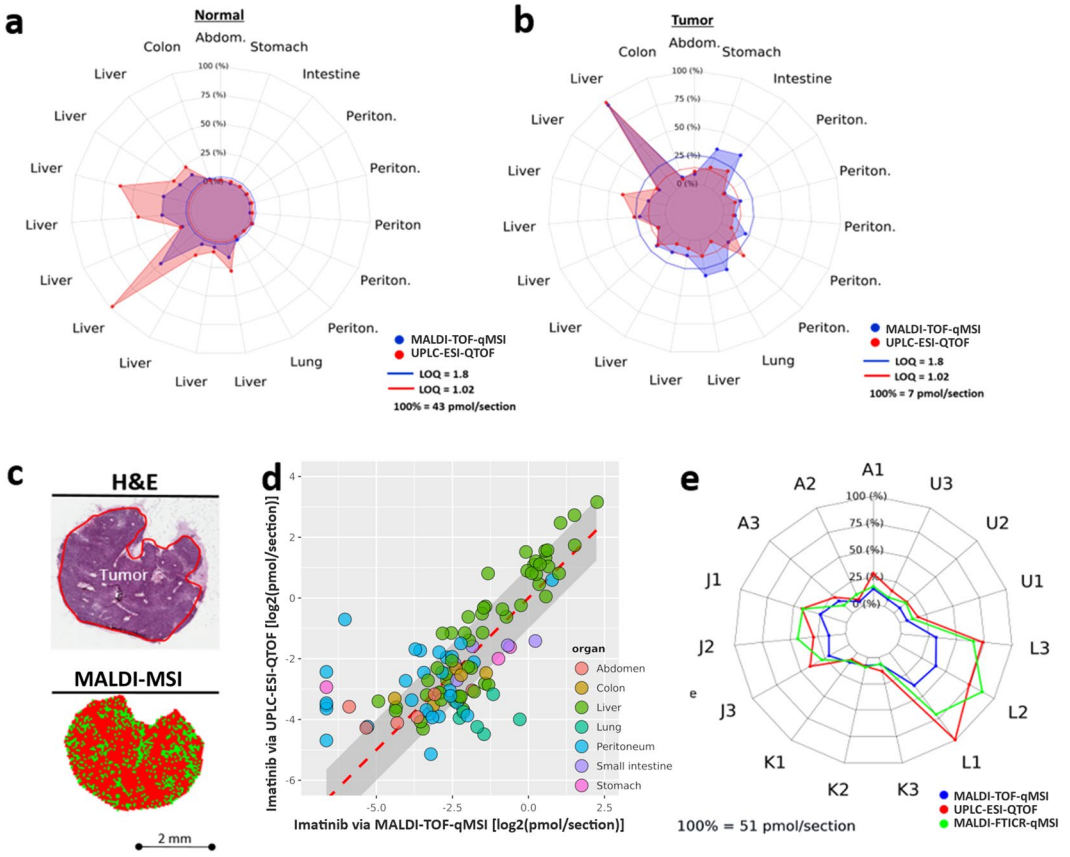

Figure 2. Verification of MALDI-TOF-qMSI for imatinib quantification in GIST. Comparison of MALDI-TOF-qMSI and UPLC-ESI-QTOF-MS quantification for (**a**) normal and (**b**) tumor tissue. (**c**) A liver metastasis (sample J) illustrating the drug-containing pixels (bottom) and corresponding H&E-stained image (top). (**d**) A correlation plot showing MALDI-TOF-qMSI on the *x*-axis and UPLC-ESI-QTOF-MS on the *y*-axis, both $\log_2$-scaled. The dashed red line represents an identity line (1:1 line) with the $\log_2$ fold change of 1 represented by the grey area around it. (**e**) Comparison of MALDI-TOF-qMSI, UPLC-ESI-QTOF-MS and MALDI-FTICR-qMSI quantification for five (x3) unaffected liver samples.

spatial information puts constraints on UPLC-ESI-QTOF-MS measurements of "tumor tissue", which are always skewed by tissue heterogeneity, i.e. the presence of unknown fractions of non-tumor tissues in tumor samples. Sample A, for which UPLC-ESI-QTOF-MS showed similar levels of imatinib in normal and tumor tissue, serves as point in case (Supplementary Fig. S7), which was explained by H&E annotation and MALDI-TOF-qMSI images (Supplementary Fig. S8). Moreover, even though MALDI-TOF- and -FTICR-qMSI has been traditionally referenced to UPLC-ESI-QTOF-MS as gold standard for absolute quantification, such validation by UPLC-ESI-QTOF-MS needs to be considered carefully, since MALDI-qMSI reports pixel-wise quantification of a few nm thin surface layer[30], while the latter quantifies the drug within a defined tissue volume.

Limited imatinib uptake in metastatic GIST independent of mutation status. To be effective, cancer-targeting drugs must adequately penetrate into tissue. Hence, we sought to investigate imatinib's tumor penetration capability in human GIST samples. Figure 3 illustrates an overview of the measured tissue sections for all 27 patient samples, done in triplicates, with green and red pixels indicating detected ($S/N \geq 3$) and undetectable drug signal, respectively (also see Supplementary Tables S1 and S2 for clinical and histopathological information and Supplementary Fig. S2 for an overview of the H&E-stained sections). Follow up histopathological examination suggested that 26 of the tumor tissue replicates examined contained only slight traces of regressive tumor areas with fibrosis and necrotic tissue throughout. They were, therefore, omitted from further analysis.

Systematic quantification of imatinib (pmol/section) in tumor tissue sections and their corresponding non-tumor (normal) control tissues by MALDI-TOF-qMSI revealed that despite continuous administration of the prescribed dosage of imatinib until surgery (see Supplementary Table S1), tissue drug levels were typically below LOQ (Fig. 4a; but see sample AA as an exception). In most tumor sections (48 of 60 sections; 80%, in MALDI-TOF-qMSI and 31 of 44; 70%, in UPLC-ESI-QTOF-MS), regardless of its type (i.e. primary tumor or metastasis) and mutation status, imatinib content was below LOQ. In comparison, for the corresponding normal tissue sections only 40 of 83 sections (48%) and 23 of 54 sections (43%) contained imatinib amounts below LOQ for MALDI-TOF-qMSI and UPLC-ESI-QTOF-MS, respectively. Imatinib levels were higher in normal liver tissues compared to the others.

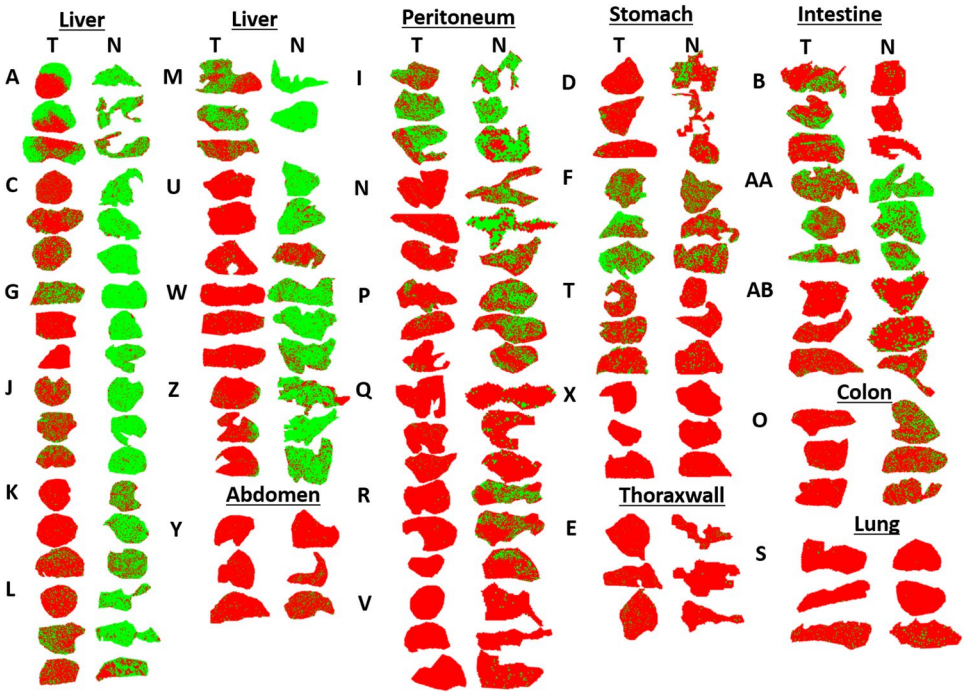

Figure 3. Imatinib distribution in all tumor (T) and normal (N) non-tumor samples from GIST patients (not to scale). Green and red pixels indicate imatinib signal presence (S/N $\geq$ 3) and absence, respectively. Three cryosections were prepared per tissue sample/patient, and samples are coded by single or double letters. Tissues identified as stomach, colon or intestine are primary tumors. All others were metastases.

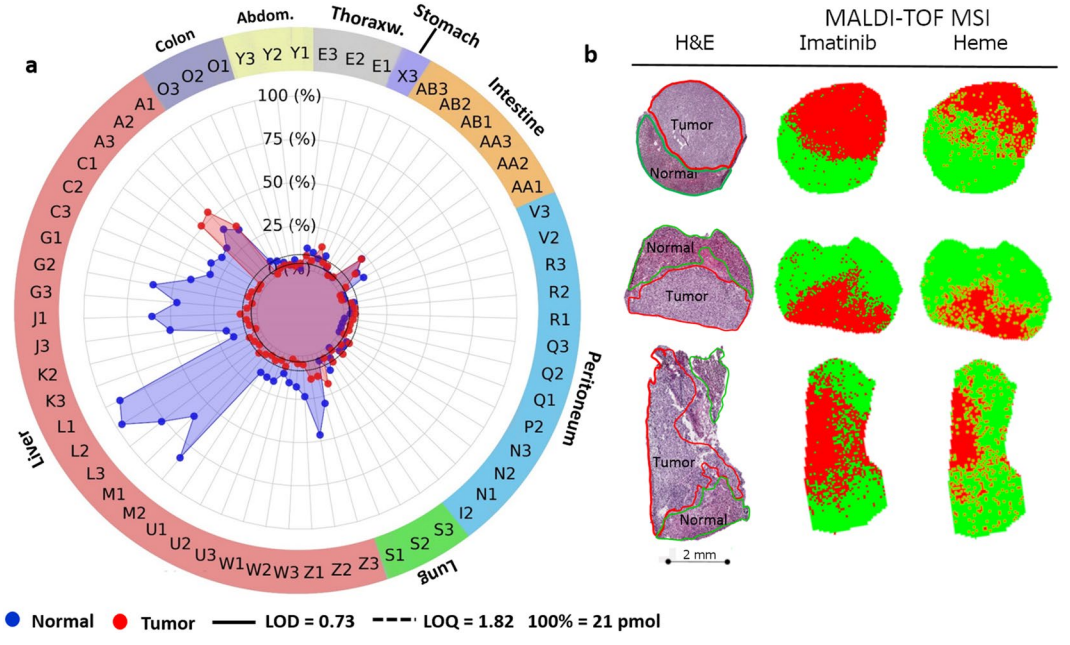

Figure 4. Liver metastases of GIST display limited imatinib content independent of mutation status. (**a**) MALDI-TOF-qMSI-Quantified imatinib in GIST samples cohort comparing "Tumor" (red) and corresponding "Normal" (blue) tissues. (LOD = 0.73 pmol/section; LOQ = 1.82 pmol/section.) (**b**) Three sample A replicates containing both "normal" and "tumor" tissue based on histopathological re-examination (left column) illustrating imatinib's absence from metastatic GIST (central column; red pixels) in addition to the heme signal detection maps (right column; green pixels: signal present; red pixels: signal absent).

Surprisingly though, the orally administered imatinib had limited uptake or retention in metastatic GIST in liver tissue, leading to amounts below LOQ despite the high abundance of the drug (well above LOQ) within surrounding normal liver tissue. Sample A appears to be a notable exception, as comparable amounts of imatinib were present in both normal and tumor tissue (also observed with UPLC-ESI-QTOF-MS in Supplementary Fig. S7). However, upon histopathological re-investigation, all three replicates of that sample were found to contain both normal hepatic and metastatic GIST tissues (Fig. 4b). As revealed by spatially-resolved-qMSI, also this sample contained imatinib only in its non-tumor part (Fig. 4b). Apparently, the drug was unable to penetrate into the metastatic tumor despite high concentrations within the surrounding tissue. Additionally, to rule out the possibility that the drug has been completely metabolized within tumor areas, N-desmethylimatinib (*m/z* 480.25), a known metabolite of imatinib[31], was detected and visualized (Supplementary Fig. S8) for the same sample described above. N-desmethylimatinib showed clear colocalization with imatinib mainly visible outside the tumor areas in normal liver tissue. Moreover, ion intensity maps for the sodium and potassium adducts of imatinib (Supplementary Fig. S9) further support this observation by showing that the absence of the targeted drug is not caused by differential tissue-dependent adduct formations. To rule out the possibility that observed differences in imatinib signal were simply a consequence of different desorption/ionization characteristics of the respective tissues, we calculated TEC for all normal tissue-tumor tissue pairs (Supplementary Fig. S5): Importantly, for liver, stomach and lung no significant differences between the drug's ionization for normal and corresponding tumor tissue were observed. Additionally, no other interfering analytes were detected within 100 ppm of imatinib as verified by high mass resolution MALDI-FTICR-MSI as shown in Supplementary Fig. S6. Hence, MALDI-TOF-qMSI results reflect real differences in drug distribution.

The observed discrepancy between imatinib amounts in normal hepatic versus metastatic tissue is striking (e.g. replicates of sample A (Fig. 4b)). Further work is required to elucidate if lack of imatinib in liver metastases reflects effective export/metabolism or inefficient uptake. For instance, higher expression of P-glycoprotein and multi-resistance protein 1 (MRP1), which are involved in active efflux of a wide spectrum of drugs including imatinib, have been reported in gastric and non-gastric GISTs, respectively[32]. Other reasons for such drug-resistance that is independent of the KIT and PDGFRA mutation status include a poorly organized vasculature, increased interstitial fluid caused by the lack of functional lymphatics and/or inflammation and abnormal structures of the extracellular matrix[14,15]. However, it has been reported elsewhere that tumor vascularity decreases in GIST metastases after treatment with imatinib[33,34]. To investigate this, we opted to visualize Heme B (*m/z* 616.17), a proven MALDI-MSI marker of vasculature (Fig. 4B, right column)[35]. Heme B imaging suggested decreased vasculature within the tumor core when compared with the surrounding hepatic tissue. Although the Heme B ion intensity map of Fig. 4b suggested vascularization that perturbs the visible boundaries of the tumor area, the actual signal intensities for Heme B within the tumor boundaries were substantially lower than those of the normal tissue (Supplementary Fig. S8). This reduction in vascularization as a result of treatment may lay the basis for subsequent tumor progression due to inadequate local drug concentrations within targeted tissues. The observed apparent lack of drug also confirms the clinical practice for GIST patients with liver metastases that the best treatment option is a multidisciplinary one with continued TKI drug therapy and possibly surgical intervention[36]. The results shown in this study (lack of drug presence in tumor), based on a small cohort of patient-derived tissues, are in line with results from several MALDI-qMSI mouse studies on various chemotherapeutic drug agents in different cell line-based and patient-derived xenograft models[18,19,21,37–39]. It should be noted that while the presence of sufficient quantities of a drug in the target tissue is invariably a prerequisite for its efficacy, MSI in clinical pharmacology may not be limited to drug distribution studies. In the future, it may be even more intriguing to use MSI for spatial assessment of drug-response markers. For instance, in a preclinical rodent model of gastric cancer we have demonstrated earlier that polyacetylated histone H4 can be imaged by MS as a pharmacodynamic marker of action of the histone deacetylase inhibitor panobinostat[40].

In summary, while providing additional spatial information on imatinib distribution, MALDI-qMSI based on generalized nonlinear calibration and focused computational analysis of drug-bearing pixels provided quantitative measures of imatinib that deviated from reference analysis by UPLC-ESI-QTOF-MS by less than two-fold in 78% of cases (87% of cases by FTICR) and provided a generalized method for modeling analytes dilution series as well as assessing the degree of the apparent nonlinearity of the system. While further refinement of the method and testing in larger patient cohorts will be crucial, our data provides a proof-of-concept for clinical utility of MALDI-qMSI. Furthermore, spatial mapping of imatinib distribution within GIST patient tissues revealed striking inefficiency in its penetration into liver metastases irrespective of their mutation status. Our study therefore strongly suggests that also mechanisms other than driver mutations in receptor tyrosine kinases such as alterations in drug uptake due to decreased intra-tumor vasculature may play an important role in imatinib resistance in GIST. This finding underlines the important application of MALDI-qMSI, a methodology that can probably be translated to clinical drugs other than the proof-of-concept case imatinib, for studying the spatial distribution of molecularly targeted therapeutics in oncology. More specifically, MALDI-qMSI can enter clinical application as an orthogonal post-surgical approach to evaluate disposition of administered drugs and their metabolites in resected specimens to cast light into possible treatment resistance as a function of anticancer drug uptake, metabolism and/or retention.

Methods

Tissue samples. Human GIST and corresponding non-tumor control tissues (total of 56 specimens) had been surgically removed from 27 patients (Supplementary Table S1) after obtaining their informed consent and approval by the Medical Ethics Committee II of the Medical Faculty Mannheim of Heidelberg University (2012-289N-MA; 2015-868R-MA; 2017-806R-MA) and was carried out in accordance with guidelines and regulations. All patients had been treated with 400–800 mg imatinib orally once daily including the day prior to surgery, hence, tumor and healthy tissue samples were analyzed at a steady state drug status before surgery. After removal,

tumor tissues was cut into small pieces, snap-frozen and stored at −80 °C in the biobank of the Department of Surgery at University Hospital Mannheim. For all samples, histology, mitotic activity, regression index and CD117 (=KIT), CD34 as well as DOG1 immunohistochemistry (IHC) were assessed. Exons 9, 11, 13, 14 and 17 of the KIT gene as well as exons 12 and 18 of the PDGFRA gene were analyzed for mutations after tumor tissue microdissection. Porcine liver tissue was used to establish drug calibration curves on test slides. These were supplied by the local slaughterhouse and immediately snap-frozen (−80 °C).

Experimental workflow and tissue preparation. Each sample was sectioned in six steps at −20 °C in a CM 1950 cryostat (Leica Biosystems GmbH, Nussloch, Germany) in triplicate (see Supplementary Fig. S1). After trimming, the first 8-µm tissue section of each sample was thaw-mounted onto a gold target for MALDI-TOF-qMSI. Two consecutive slices were then put onto Starfrost adhesive microscope slides (R. Langenbrinck GmbH, Emmendingen, Germany) for standard histological analysis (one stained with hematoxylin & eosin (H&E) and one backup slide) and scanned in an Aperio CS2 (Leica Biosystems). Afterwards, four consecutive sections were collected for quantitative drug determination by UPLC-ESI-QTOF-MS. Finally, some exemplary sections were mounted on conductive indium tin oxide (ITO) slides for additional MALDI-qMSI with a high mass-resolving FTICR-MS (n = 3). For MALDI-qMSI, each ITO slide featured duplicate spots of an imatinib dilution series (25, 12.5, 6.25, 3.125, 1.56, 0.78 pmol and a blank control) spotted onto a porcine liver section. For a schematic overview of the arrangement of tissue sections on slides, see Supplementary Fig. S1. To achieve comparable conditions after preparation, all slides were stored in a desiccator at room temperature for one hour.

Quantitative MALDI-TOF- and -FTICR imaging. For normalization, nine layers of deuterated imatinib (imatinib-D8) were deposited on the slides using a SunCollect sprayer (SunChrom GmbH, Friedrichsdorf, Germany): 2.5 pmol/µL solution, flow rate 15 µL/min, spray head distance 45 mm and speed 300 mm/min. Slides were stored in a desiccator at room temperature for one hour to allow drying of the IS. For positive-ion mode measurements, five layers (flow rates of 10, 15, 3 × 20 µL/min) of 2,5-Dihydroxybenzoic acid (DHB) matrix (60 mg/mL in 50% acetonitrile, 0.5% Trifluoroacetic acid) were subsequently sprayed onto the tissue at 300 mm/min as described previously[41].

MALDI-TOF-qMSI data acquisition was performed on an ultrafleXtreme MS using flexControl 3.4 (Bruker Daltonics GmbH; for instrument parameters, see Supplementary Methods). High-resolving-power MSI (*m/z* 150–3000; R: 260,000 at *m/z* 300) was recorded in positive-ion mode on a solariX 7T XR FTICR mass spectrometer (Bruker Daltonics). The raster width was 200 µm for calibration curves for quantification and 50 µm for all human samples. The instrument was calibrated externally using quadratic mass calibration with peptide calibration standard II including dasatinib (*m/z* 488.21). For imatinib calibration curves, equal square-sized measurement areas containing identical pixel numbers were defined over each calibration spot by an in-house MATLAB tool.

Data import, conversion and preprocessing. A total of 48 MALDI-TOF- and three MALDI-FTICR-qMSI-datasets were acquired and exported into imzML format[42] using flexImaging 4.1 (Bruker Daltonics) with a binning rate of 120,000. The imzML datasets were subsequently imported into R 3.3.1 (R Foundation for Statistical Computing, Vienna, Austria)[43] using MALDIquantForeign and processed using MALDIquant packages[44]. Mass spectra were normalized to the maximum peak intensity over the mass range *m/z* 502.32 ± 100 ppm (MALDI-TOF-qMSI) and ±10 ppm (MALDI-FTICR-qMSI) of the sprayed IS imatinib-D8. Neither baseline correction nor further pre-processing of spectra were performed. All subsequent analysis and visualization (mainly with ggplot2 and fmsb packages) were performed using R.

Regression models and quantification. Linear regression analysis for calibration of the spotted imatinib dilution series was performed as described in[9,10]. Nonlinear regression was performed by fitting a power function as a calibration curve in the form of $y = ax^b + c$ model (for details see Supplementary Methods; Calibration Curves). For MALDI-qMSI of imatinib in tissue, the mean intensity of signal-bearing pixels, i.e. imatinib signal with signal to noise ratio (S/N) ≥ 3, of each tissue section was plugged into the fitted nonlinear regression model. The limits of detection (LOD) and quantification (LOQ) in this study were computed as mean of all individually fitted calibration curves (48 for MALDI-TOF-qMSI and 3 for MALDI-FTICR-qMSI; see Supplementary Fig. S4). To assess imatinib ion suppression within different tissues, TEC[10] was calculated as the ratio of the mean intensity of the deuterated IS (*m/z* 502.32 ± 100 ppm) within each tissue section to its mean intensity in the IS and matrix control area. RSE was used for quality of fit comparison, as R^2 is not defined for nonlinear fits[45].

Data Availability

A subset of MALDI-FTICR-MSI and MALDI-TOF-MSI datasets of individual tissue sections is available on METASPACE[46] [https://metaspace2020.eu/]. The rest of the datasets generated and/or analyzed during the current study are not publicly available but are available from the corresponding author on reasonable request.

References

1. Ellis, S. R., Bruinen, A. L. & Heeren, R. M. A. A critical evaluation of the current state-of-the-art in quantitative imaging mass spectrometry. *Anal. Bioanal. Chem.* **406**, 1275–1289 (2014).
2. Sun, N. & Walch, A. Qualitative and quantitative mass spectrometry imaging of drugs and metabolites in tissue at therapeutic levels. *Histochemistry and Cell Biology* **140**, 93–104 (2013).
3. Rzagalinski, I. & Volmer, D. A. Quantification of low molecular weight compounds by MALDI imaging mass spectrometry – A tutorial review. *Biochimica et Biophysica Acta, Proteins and Proteomics* **1865**, 726–739 (2017).
4. Schulz, S., Becker, M., Groseclose, M. R., Schadt, S. & Hopf, C. Advanced MALDI mass spectrometry imaging in pharmaceutical research and drug development. *Curr. Opin. Biotechnol.* **55**, 51–59 (2019).

5. Swales, J. G., Hamm, G., Clench, M. R. & Goodwin, R. J. A. Mass spectrometry imaging and its application in pharmaceutical research and development: A concise review. *Int. J. Mass Spectrom.* https://doi.org/10.1016/j.ijms.2018.02.007 (2018).
6. Fülöp, A. *et al.* Molecular imaging of brain localization of liposomes in mice using MALDI mass spectrometry. *Sci. reports* **6**, 33791 (2016).
7. Karlsson, O. & Hanrieder, J. Imaging mass spectrometry in drug development and toxicology. *Arch. Toxicol.* **91**, 2283–2294 (2017).
8. Cornett, D. S., Frappier, S. L. & Caprioli, R. M. MALDI-FTICR imaging mass spectrometry of drugs and metabolites in tissue. *Anal. Chem.* **80**, 5648–5653 (2008).
9. Koeniger, S. L. *et al.* A quantitation method for mass spectrometry imaging. *Rapid Commun. Mass Spectrom.* **25**, 503–510 (2011).
10. Hamm, G. *et al.* Quantitative mass spectrometry imaging of propranolol and olanzapine using tissue extinction calculation as normalization factor. *J. Proteomics* **75**, 4952–4961 (2012).
11. Pirman, D. A., Reich, R. F., Kiss, A., Heeren, R. M. A. & Yost, R. A. Quantitative MALDI tandem mass spectrometric imaging of cocaine from brain tissue with a deuterated internal standard. *Anal. Chem.* **85**, 1081–1089 (2013).
12. Groseclose, M. R. & Castellino, S. A mimetic tissue model for the quantification of drug distributions by MALDI imaging mass spectrometry. *Anal. Chem.* **85**, 10099–10106 (2013).
13. van de Ven, S. M. W. Y. *et al.* Protein biomarkers on tissue as imaged via MALDI mass spectrometry: A systematic approach to study the limits of detection. *Proteomics* **16**, 1660–1669 (2016).
14. Minchinton, A. I. & Tannock, I. F. Drug penetration in solid tumours. *Nature Reviews Cancer* **6**, 583–592 (2006).
15. Marusyk, A. & Polyak, K. Tumor heterogeneity: Causes and consequences. *Biochimica et Biophysica Acta, Reviews on Cancer* **1805**, 105–117 (2010).
16. Carmona-Fontaine, C. *et al.* Metabolic origins of spatial organization in the tumor microenvironment. *Proc. Natl. Acad. Sci.* **114**, 2934–2939 (2017).
17. Ait-Belkacem, R. *et al.* Microenvironment Tumor Metabolic Interactions Highlighted by qMSI: Application to the Tryptophan-Kynurenine Pathway in Immuno-Oncology. *SLAS Discov. Adv. Life Sci. R&D* 247255521771265, https://doi.org/10.1177/2472555217712659 (2017).
18. Giordano, S. *et al.* 3D Mass Spectrometry Imaging Reveals a Very Heterogeneous Drug Distribution in Tumors. *Sci. Reports* **6**, 37027 (2016).
19. Tsubata, Y. *et al.* Evaluation of the heterogeneous tissue distribution of erlotinib in lung cancer using matrix-assisted laser desorption ionization mass spectrometry imaging. *Sci. Reports* **7**, 12622 (2017).
20. Nishimura, M., Hayashi, M., Mizutani, Y. & Takenaka, K. Distribution of erlotinib in rash and normal skin in cancer patients receiving erlotinib visualized by matrix assisted laser desorption / ionization mass spectrometry imaging. *Oncotarget* **9**, 18540–18547 (2018).
21. Gruner, B. M. *et al.* Modeling Therapy Response and Spatial Tissue Distribution of Erlotinib in Pancreatic Cancer. *Mol. Cancer Ther.* **15**, 1145–1152 (2016).
22. Miettinen, M. & Lasota, J. Histopathology of Gastrointestinal Stromal Tumor. *Journal of Surgical Oncology* 865–873, https://doi.org/10.1002/jso.21945 (2011).
23. Casali, P. G. *et al.* Gastrointestinal stromal tumours: ESMO–EURACAN Clinical Practice Guidelines for diagnosis, treatment and follow-up†. *Ann. Oncol.* **29**, iv68–iv78 (2018).
24. Wardelmann, E. *et al.* Polyclonal Evolution of Multiple Secondary KIT Mutations in Gastrointestinal Stromal Tumors under Treatment with Imatinib Mesylate. *Clin. Cancer Res.* **12**, 1743–1749 (2006).
25. Joensuu, H., Hohenberger, P. & Corless, C. L. Gastrointestinal stromal tumour. *The Lancet* **382**, 973–983 (2013).
26. Serrano, C. *et al.* Novel Insights into the Treatment of Imatinib-Resistant Gastrointestinal Stromal Tumors. *Target. Oncol.* **12**, 277–288 (2017).
27. Mei, L., Du, W., Idowu, M., von Mehren, M. & Boikos, S. A. Advances and Challenges on Management of Gastrointestinal Stromal Tumors. *Front. Oncol.* **8**, 135 (2018).
28. von Mehren, M. & Widmer, N. Correlations between imatinib pharmacokinetics, pharmacodynamics, adherence, and clinical response in advanced metastatic gastrointestinal stromal tumor (GIST): An emerging role for drug blood level testing? *Cancer Treat. Rev.* **37**, 291–299 (2011).
29. Heeren, R. M. A., Smith, D. F., Stauber, J., Kükrer-Kaletas, B. & MacAleese, L. Imaging Mass Spectrometry: Hype or Hope? *J. Am. Soc. Mass Spectrom.* **20**, 1006–1014 (2009).
30. Van Nuffel, S. *et al.* Insights into the MALDI Process after Matrix Deposition by Sublimation Using 3D ToF-SIMS Imaging. *Anal. Chem.* **90**, 1907–1914 (2018).
31. Friedecký, D. *et al.* Detailed study of imatinib metabolization using high-resolution mass spectrometry. *J. Chromatogr. A* **1409**, 173–181 (2015).
32. Theou, N. *et al.* Multidrug resistance proteins in gastrointestinal stromal tumors: Site-dependent expression and initial response to imatinib. *Clin. Cancer Res.* **11**, 7593–7598 (2005).
33. Lassau, N. *et al.* Gastrointestinal Stromal Tumors Treated with Imatinib: Monitoring Response with Contrast-Enhanced Sonography. *Am. J. Roentgenol.* **187**, 1267–1273 (2006).
34. Meyer, M. *et al.* CT-based response assessment of advanced gastrointestinal stromal tumor: Dual energy CT provides a more predictive imaging biomarker of clinical benefit than RECIST or Choi criteria. *Eur. J. Radiol.* **82**, 923–928 (2013).
35. Liu, X. *et al.* Molecular imaging of drug transit through the blood-brain barrier with MALDI mass spectrometry imaging. *Sci. Reports* **3**, (2013).
36. Seesing, M. F. J. *et al.* Resection of liver metastases in patients with gastrointestinal stromal tumors in the imatinib era: A nationwide retrospective study. *Eur. J. Surg. Oncol.* **42**, 1407–1413 (2016).
37. Aikawa, H. *et al.* Visualizing spatial distribution of alectinib in murine brain using quantitative mass spectrometry imaging. *Sci. Reports* **6**, (2016).
38. Giordano, S. *et al.* Heterogeneity of paclitaxel distribution in different tumor models assessed by MALDI mass spectrometry imaging. *Sci. Reports* **6** (2016).
39. Morosi, L. *et al.* Application of 3D Mass Spectrometry Imaging to TKIs. *Clin. Pharmacol. Ther.* **102**, 748–751 (2017).
40. Munteanu, B. *et al.* Label-FreeMonitoring of Histone Deacetylase Drug Target Engagement by Matrix-Assisted Laser Desorption Ionization-Mass Spectrometry Biotyping and Imaging. *Analytical Chemistry* **86**(10), 4642–4647 (2014).
41. Hinsenkamp, I. *et al.* Inhibition of Rho-Associated Kinase 1/2 Attenuates Tumor Growth in Murine Gastric Cancer. *Neoplasia (United States)* **18**, 500–511 (2016).
42. Schramm, T. *et al.* imzML — A common data format for the flexible exchange and processing of mass spectrometry imaging data. *J. Proteomics* **75**, 5106–5110 (2012).
43. Ihaka, R. & Gentleman, R. R: A Language for Data Analysis and Graphics. *J. Comput. Graph. Stat.* **5**, 299–314 (1996).
44. Gibb, S. & Strimmer, K. MALDIquant: a versatile R package for the analysis of mass spectrometry data. *Bioinformatics* **28**, 2270–2271 (2012).
45. Spiess, A.-N. & Neumeyer, N. An evaluation of R2 as an inadequate measure for nonlinear models in pharmacological and biochemical research: a Monte Carlo approach. *BMC Pharmacol.* **10**, 6 (2010).
46. Palmer, A. *et al.* FDR-controlled metabolite annotation for high-resolution imaging mass spectrometry. *Nat. Methods* **14**, 57–60 (2016).

Acknowledgements

This work was supported by the European Union's Seventh Framework Programme (FP7/2007–2013) under grant agreement no. 602306 (MITIGATE; to C.H.). This research project was also funded by the German Federal Ministry of Education and Research (BMBF) within the Framework "Forschungscampus: public-private partnership for Innovations" (M^2oBiTE grant 13GW0091B to C.H. and 13GW0091E to A.M.). The authors thank Karin Berner-Leischner for technical assistance with the tissue samples. Eva Wardelmann, Dept. of Pathology, University Hospital Münster was instrumental in analyzing secondary resistance mutations. C.H. thanks the Deutsche Forschungsgemeinschaft (DFG) for the funding of a SolariX FTICR MS (INST 874/7-1 FUGG). An earlier version of this manuscript was posted as a preprint on bioRxiv (https://doi.org/10.1101/562553).

Author Contributions

D.A.S., C.M., C.H. wrote the article; D.A.S., C.M., A.G., K.E., S.S., J.H.R., P.F., C.H. designed the research; P.H. conceptualized the clinical study design incl. treatment of patients with imatinib prior to surgery and provided clinical samples. C.M., A.G., K.E., S.S., C.R.G., J.H.R., performed the research; D.A.S., C.M., A.G. and C.H. analyzed analytical data; A.M. analyzed histopathological specimens and data.

Additional Information

Supplementary information accompanies this paper at https://doi.org/10.1038/s41598-019-47089-5.

Competing Interests: The authors declare no competing interests.

Publisher's note: Springer Nature remains neutral with regard to jurisdictional claims in published maps and institutional affiliations.